



## Pharmaceutical Biotechnology

## Raman Marker Bands for Secondary Structure Changes of Frozen Therapeutic Monoclonal Antibody Formulations During Thawing

Astrid Hauptmann<sup>a</sup>, Georg Hoelzl<sup>a</sup>, Martin Mueller<sup>a</sup>, Karoline Bechtold-Peters<sup>b</sup>, Thomas Loerting<sup>c,\*</sup><sup>a</sup> Sandoz GmbH, 6336, Langkampfen, Austria<sup>b</sup> Novartis Pharma AG, 4057, Basel, Switzerland<sup>c</sup> Institute of Physical Chemistry, University Innsbruck, Innsbruck, Austria

## ARTICLE INFO

## Article history:

Received 21 August 2022

Revised 16 October 2022

Accepted 16 October 2022

Available online 22 October 2022

## Keywords:

Raman spectroscopy

Frozen mab solutions

Freeze and thaw damage

Aggregation

Formulation

Tyrosine ratio

Secondary structure

Tertiary structure

## ABSTRACT

In this work we use Raman spectroscopy for protein characterization in the frozen state. We investigate the behavior of frozen therapeutic monoclonal antibody IgG1 formulation upon thawing by Raman spectroscopy. Secondary and tertiary structure of the protein in three different mab formulations in the frozen state are followed through observation of marker bands for  $\alpha$ -helix,  $\beta$ -sheet and random coil. We identify the tyrosine intensity ratio  $I_{856}/I_{830}$  as a marker for mab aggregation. Upon fast cooling (40 °C/min) to –80 °C we observe a significant increase of random coil and  $\alpha$  –helical structures, while this is not the case for slower cooling (20 °C/min) to –80 °C. Most changes in the protein's secondary structure are observed in the course of thawing in the range up to –20 °C, when passing through the glass transitions and cold-crystallization of the two types of freeze-concentrated solutions formed through macro- and microcryoconcentration. An increase of protein concentration and the addition of mannitol suppress secondary structural changes but do no impact on aggregation.

© 2022 The Authors. Published by Elsevier Inc. on behalf of American Pharmacists Association. This is an open access article under the CC BY license (<http://creativecommons.org/licenses/by/4.0/>)

## Introduction

The freezing and thawing (FT) process plays an important role in the manufacturing, transportation and storage of pharmaceutical products. Even though it is commonly applied to avoid or limit foam production, mechanical stress, restricting microbial growth and to increase the shelf-life,<sup>1</sup> the process itself still comes with challenges for pharmaceutical industries (e.g. crystallization of excipients, pH-shifts, stress at ice-liquid interfaces and cryoconcentration). Hereby, the highest and utmost priority lies in the preservation and protection of the protein in order to ensure the quality and safety of the product. Therapeutic protein solutions, including monoclonal antibody (mab) solutions, may suffer from structural changes during FT processes. These structural changes can cause misfolding/unfolding,<sup>2,3</sup> leading to protein aggregation and in - the worst-case - loss of biological activity and/or an increase of immunogenic response in patients.<sup>4–6</sup> Various aggregation pathways have been reported in literature.<sup>7</sup>

FT stress may contribute to structural changes of proteins, e.g., through cryoconcentration, phase separation,<sup>8</sup> surface-induced denaturation<sup>9–11</sup> or change of chemical micro-environment caused by buffer salts or cryoprotectants. Freezing and storage protocols that have a set-point temperature below all glass transition temperatures ( $T_g$  and  $T_g'$ ) are preferred to avoid ice crystallization or molecular mobility is likely.<sup>12,13</sup> Cryoprotectants can be helpful to minimize the damaging effects of FT on the protein<sup>2,14–16</sup> in aqueous solutions<sup>12,17,18</sup>. Hereby, the formulation plays a decisive role. Buffer formulations have to be properly characterized for their impact on  $T_g'$  which depends on type of cryoprotectants, concentration of excipients, pH value and ionic strength.<sup>19–23</sup>

In our study, we demonstrate the power of Raman spectroscopy for the characterization of the secondary and tertiary structure of mab formulations during FT. Raman bands carry information about the local chemical environment, e.g., functional groups. In aqueous solutions, band patterns are specific for solutes and their hydration. They differ significantly in liquid solution, in glassy solution or in the crystalline state. Also, monomers, dimers and higher oligomers of solutes can be distinguished. Band intensities may be used as an indicator for the concentration of certain species, e.g., monomeric or

\* Corresponding author at: Innrain 52c, 6020, Innsbruck, Austria.

E-mail address: [thomas.loerting@uibk.ac.at](mailto:thomas.loerting@uibk.ac.at) (T. Loerting).

aggregated proteins. The linewidth of the bands provides information about order, e.g., crystalline versus amorphous nature of a solid sample.

This concept is illustrated in the Fig. 1 on the example of peptides.<sup>24</sup> Changes of secondary structure can be inferred from 9 characteristic amide bands associated with the CONH group: Amide A (3225–3280  $\text{cm}^{-1}$ ),<sup>25</sup> B and I–VII bands (in order of decreasing wavenumbers). The so called “fingerprint region” contains Amide I–III (see Fig. 1, right and Table 1).

Since a mab formulation consists of protein in aqueous buffer, the most prominent peak, the O–H-stretch at 3130  $\text{cm}^{-1}$ , can be used as an indicator for presence of buffer solution (see Fig. 1, left). Amide I–III are commonly used for characterizing changes of secondary structure in proteins<sup>33–35</sup> since the carbonyl (C=O) and the amine (N–H) groups on the protein backbone (see Fig. 1, left, inset) contribute to hydrogen bonding in  $\alpha$ -helix,  $\beta$ -sheet and random coil.<sup>36</sup> A native IgG antibody consists mainly of  $\beta$ -sheets.<sup>37,38</sup> Depending on the network of the stabilizing hydrogen bonds (N–H...O=C) in between adjacent  $\beta$ -strands, a  $\beta$ -sheet can be categorized into antiparallel and parallel.<sup>31</sup> IgG antibodies only consist of antiparallel  $\beta$ -sheets. In particular, an IgG antibody shows 12 domains (8 domains in the Fab region and 4 in the Fc region). Each constant domain consists of 7 antiparallel  $\beta$ -strands and each variable domain counts 7+2 antiparallel  $\beta$ -strands. The  $\beta$ -strands are arranged in 2  $\beta$ -sheets stabilized by one disulfide bridge.

Random coil means that the protein does not show a specific secondary structure but rather a random orientation of amino acids with inherent local interactions.<sup>39</sup>

The tertiary structure of any protein is inferred based on disulfide bridges and aromatic amino acids of the side chains. The disulfide bond band is seen in the Raman spectra between 500  $\text{cm}^{-1}$  and 550  $\text{cm}^{-1}$  depending on the conformation, the mode of coupling and the hydrogen bonds.<sup>40</sup> The aromatic residues of amino acids phenylalanine (Phe), tryptophan (Trp) and tyrosine (Tyr) cause many vibrational bands in the fingerprint region (600–1800  $\text{cm}^{-1}$ ) as listed in Table 2. Due to their high sensitivity to the chemical environment, wavenumbers may shift by 5  $\text{cm}^{-1}$ .

The tyrosine (Tyr) doublet of IgG at 830  $\text{cm}^{-1}$  and 856  $\text{cm}^{-1}$  is given attention since the band intensity ratio (856  $\text{cm}^{-1}$ )/(830  $\text{cm}^{-1}$ ) is important indicator reflecting the degree of “exposure” to the solvent. The polar uncharged amino acid tyrosine is a proton donor or acceptor. Hence, tyrosine forms hydrogen bonds either within the

protein (both main chain and side chain) when being buried or with the water molecules of the solvent (here buffer solution) or other tyrosine residues of adjacent antibodies when being exposed. Hydrophobic amino acids, in contrast, are usually buried inside the protein core with limited to no access to the aqueous solvent. When tyrosine is exposed the surface area of the residue in the protein structure in contact with the buffer solution increases. Thus, if the intensity ratio (856  $\text{cm}^{-1}$ )/(830  $\text{cm}^{-1}$ ) is above 1 the hydroxyl group of tyrosine is exposed to the buffer solution, and acts as a H-bond acceptor. By contrast, if the ratio is below 1 the OH group acts as a hydrogen-bond donor and is buried<sup>44</sup> within the protein structure.<sup>45</sup> That is, the intensity ratio is also known as a marker for hydration<sup>46</sup> and a marker for tyrosine side chain interaction<sup>47</sup> (e.g., with  $\text{NH}_3^+$  groups of other amino acids). Tyrosine residues in IgG are part of the Fab region which can be expected to interact with other tyrosine residues of neighboring IgG<sup>42,48</sup> (dityrosine formation). Hence, the tyrosine intensity ratio is suitable as a marker for possible aggregation.<sup>42</sup> Additionally, the band assigned to phenylalanine at around 1000  $\text{cm}^{-1}$  has been suggested as a pre-aggregation marker.<sup>42</sup> In the scientific community the phenylalanine band is also known and commonly used as an internal standard since it is not sensitive to protein conformation or microenvironment.<sup>49,50</sup> At the same time this band can indicate the extent of deamidation in protein.<sup>49</sup>

In this work we qualitatively investigate structural changes of a frozen monoclonal antibody (mab) during thawing with a focus on the secondary ( $\beta$ -sheets,  $\alpha$ -helix and random coil) and tertiary structural changes of three different mab formulations. Concentration and composition of the formulation is varied during the study.

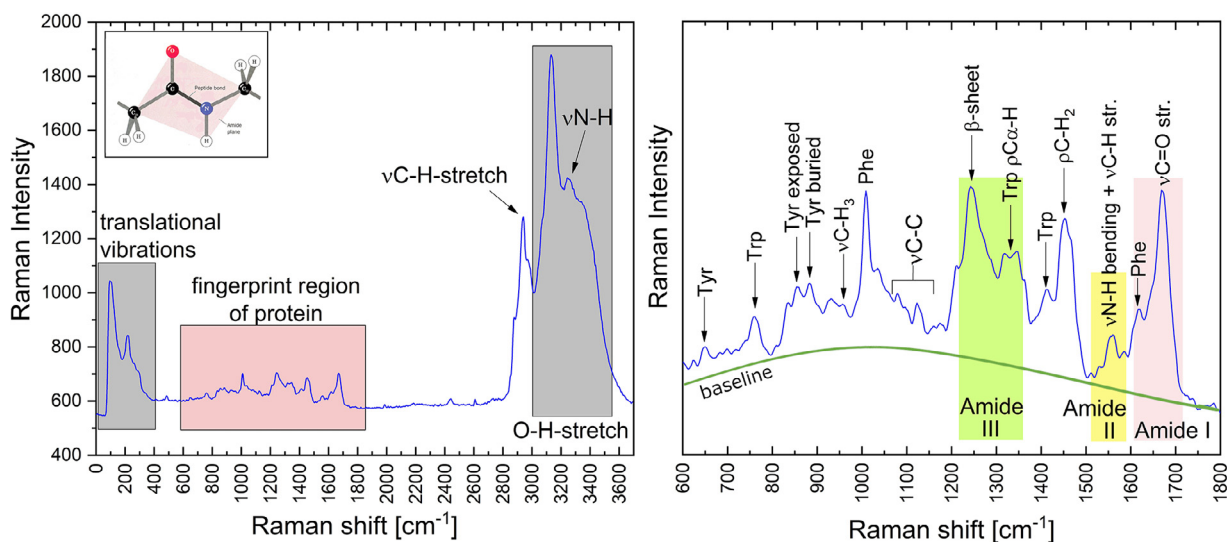
## Material and Methods

### Sample Preparation

Mab formulations 1, 2 and 3 contain the same concentration of buffer but different concentrations of protein. Mab formulation 3 contains mannitol as a cryoprotectant.

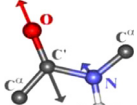
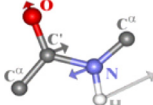
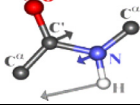
The protein consisting of a human IgG1 antibody was formulated in:

- Formulation 1 = 95.2 mg/ml mab in 22.5mM adipic acid buffer
- Formulation 2 = 163 mg/ml mab in 22.5mM adipic acid buffer



**Figure 1.** (left) Full Raman spectrum and (right) fingerprint region of a frozen IgG1 mab formulation taken at  $-40^\circ\text{C}$ .<sup>26</sup>

**Table 1**Literature assignments for Amide I–III Raman bands. Chemical structures taken from reference<sup>24</sup> and assignments taken from references.<sup>27–32</sup>

Band	Position [cm <sup>-1</sup> ]	Assignment	Structure	Structural Characteristics (wavenumbers vary in literature)
Amide I	1650	80% C=O stretch 10% N-H bend 10% N-C stretch		$\alpha$ -helix unordered. + random coil 1620 cm <sup>-1</sup> $\alpha$ -helix ordered 1640–1655 cm <sup>-1</sup> Antiparallel $\beta$ -strand 1670–1690 cm <sup>-1</sup> Parallel $\beta$ -strand 1650–1675 cm <sup>-1</sup>
Amide II	1550	60% $\delta$ (N-H) bend and 40% $\nu$ (N-C) stretch		Parallel and antiparallel $\beta$ -sheet (very weak)
Amide III	1300	40% $\nu$ (N-C) stretch and 30% $\delta$ (N-H) bend + skeleton stretches		$\alpha$ -helix 1265–1300 cm <sup>-1</sup> $\beta$ -sheet 1229–1235 cm <sup>-1</sup> random coil 1243–1253 cm <sup>-1</sup>

- Formulation 3 = 164.5 mg/ml mab in 22.5mM adipic acid buffer and 42 mg/ml mannitol

In order to validate the use of the tyrosine ratio  $I_{856}/I_{830}$  as a marker of aggregation, we were shaking mab formulation 1 in a thermomixer at 2000 rpm at a temperature of 55 °C for 72 hours prior measurement. The formulation then contains a high number of aggregates and was analyzed using Raman spectroscopy.

#### Raman Spectroscopy

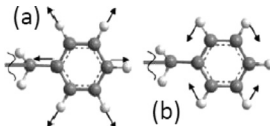
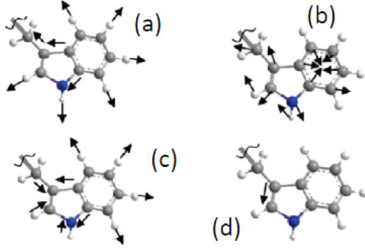
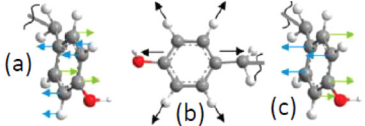
The Raman instrument (WITec GmbH, Germany) was equipped with a monochromatic light source consisting of a green laser with an excitation wavelength of 532 nm. Before every Raman spectroscopy measurement, the monochromator of the spectrometer was calibrated by using the Stokes line of a silicon wafer at 513 cm<sup>-1</sup> (at 20 °C). We used a 10x microscope objective (Olympus MPlan) and a 600 lines/mm grating or alternatively a 40 × (Zeiss LDPlan-NEO-FLUAR) and a 50 × (Olympus LMPanFI) objective. All three objectives have a high numerical aperture, which means a high light-gathering ability and resolution.

Temperature was controlled using the cryostage LTS420 (Linkam Scientific Instruments, UK) by pumping liquid nitrogen (LN<sub>2</sub>) into the chamber.

For sample measurements, a droplet (approximately 1–2  $\mu$ l) was placed on the glass objective slide and cooled to –80 °C in the cryostage applying cooling and heating rates of 40 °C/min and 20 °C/min. Before starting the measurement, a visible inspection of the sample through the microscope allows to find the best possible spot for measurements in terms of focal point. The CCD (charge-coupled device) detector consisting of an array of light-sensitive Si-photodiodes detects the photons, which are plotted as CCD counts against the wavenumber. For large area scans a certain area in the sample was selected within the droplet and several single Raman spectra were recorded within the area.

Data preparation consisted of removing the cosmic rays (filter size 4, dynamic factor 2) and reduction of noise by applying a Savitzky-Golay filter (also known as DISPO - digital smoothing polynomial-filter) using the spectroscopic software (WITec Suite Project FOUR 4.1, WITec GmbH, Germany). Hereby we chose the following filter parameters: left 4 points, right 4 points, polynomial function of the second order, derivative 0. Spectral data of frozen sample were normalized

**Table 2**Selected Raman spectroscopy modes of aromatic amino acids in the "fingerprint region". Valence structures taken from Reference.<sup>41</sup> Raman spectroscopy shifts are collected from several publications.<sup>32,42,43</sup>

Amino acid	Assignment and wavenumbers [cm <sup>-1</sup> ]	Structure
Phe	Symmetric breathing mode 1005 cm <sup>-1</sup> (a) In-plane ring C-H bending mode 1030 cm <sup>-1</sup> (b) Also at 620 cm <sup>-1</sup> , 1584 cm <sup>-1</sup> and 1605 cm <sup>-1</sup>	
Trp	Symmetric benzene/pyrrole in-phase breathing mode 755 cm <sup>-1</sup> (a) Indole ring vibration with NH bending mode 880 cm <sup>-1</sup> (b) Symmetric benzene/pyrrole out-of-phase breathing mode 1011 cm <sup>-1</sup> (c) Pyrrole C2-C3 stretching mode 1550 cm <sup>-1</sup> (d) Also at 1584 cm <sup>-1</sup> and between 1340–1360 cm <sup>-1</sup>	
Tyr	Symmetric ring breathing mode 640 cm <sup>-1</sup> (a) In plane ring breathing mode 830 cm <sup>-1</sup> (b) Out-of-plane ring bending mode 856 cm <sup>-1</sup> (c) skeletal tyrosine 647 cm <sup>-1</sup> and 758 cm <sup>-1</sup>	

against the OH-stretching band of ice at around  $3200\text{ cm}^{-1}$  except for spectra that were recorded of the aggregated samples.

### Differential Scanning Calorimetry (DSC)

Approximately 25–30 mg of mab formulation 1 containing adipic acid buffer was loaded into an aluminum crucible which was hermetically sealed with a cover lid and transferred to the DSC 8000 device (Perkin-Elmer, USA). The sample was cooled to  $-80\text{ }^{\circ}\text{C}$  at a cooling rate of  $60\text{ }^{\circ}\text{C}/\text{min}$ , equilibrated for 5 minutes at that temperature and reheated at  $60\text{ }^{\circ}\text{C}/\text{min}$  to  $5\text{ }^{\circ}\text{C}$ . Prior to the measurements the DSC instrument was calibrated using the recommended transitions in cyclopentane, cyclohexane, indium, and adamantane to ensure correct transformation temperature at subzero temperatures with an accuracy of  $\pm 0.5\text{ }^{\circ}\text{C}$ .<sup>18</sup>

### Optical Cryomicroscopy

Images of droplets containing mab formulation 1 in emulsion (halocarbon oil/lanoline emulsion)<sup>51</sup> were taken using an optical microscope BX-51 (Olympus Corporation, Japan). The temperature was controlled by a Linkam cryostage LTS420 (Linkam Scientific Instruments, UK). As a cooling medium liquid nitrogen was used. Sample was placed on an object glass plate and positioned in the cryo-chamber at ambient temperature. After closing the cryo-chamber the droplet was cooled to  $-80\text{ }^{\circ}\text{C}$  at a rate of  $5\text{ }^{\circ}\text{C}/\text{min}$  and reheated at a rate of  $5\text{ }^{\circ}\text{C}/\text{min}$ . Microscopic images were taken by using standard transmitted light with an ULWD 10x objective (Olympus).

## Results

### Calorimetric and Optical Information on Glass Transitions and Cold-Crystallization Events

Calorimetry scans show three thermal events upon heating mab formulation 1 at  $60\text{ }^{\circ}\text{C}/\text{min}$  (marked by arrows and circle in Fig. 2, left) on top of the massive ice melting endotherm. Optical inspection using the cryomicroscope helps to assign the circled thermal event to cold-crystallization at around  $-22\text{ }^{\circ}\text{C}$ . Cold-crystallization refers to a crystallization event that takes places upon heating. Cold-crystallization of mab formulation is seen as a sudden darkening of droplets

(see areas marked by yellow circles in Fig. 2, right). The two thermal events marked by arrows are two glass transitions, one at  $-58\text{ }^{\circ}\text{C}$  and one at  $-48\text{ }^{\circ}\text{C}$ , respectively. These temperatures were obtained for heating rates of  $60\text{ }^{\circ}\text{C}/\text{min}$  and need to be corrected for thermal lag. Without thermal lag both  $T_g$ 's are lower by about  $5\text{ }^{\circ}\text{C}$ .

### RAMAN Spectroscopy

#### Influence of Cooling and Heating Rate on The Secondary Structure of Mab Formulation 1

Direct cooling to  $-80\text{ }^{\circ}\text{C}$  at a rate of  $40\text{ }^{\circ}\text{C}/\text{min}$  results in a change of secondary mab structure as evidenced in Fig. 3, blue trace. The marker bands for random coil at  $1251\text{ cm}^{-1}$  and  $\alpha$ -helix at  $1270\text{ cm}^{-1}$  and  $1635\text{ cm}^{-1}$  increase (marked by random coil and  $\alpha$  in Fig. 2). Furthermore, also the intensity of the phenylalanine band at  $1008\text{ cm}^{-1}$  increases significantly in comparison to native mab in the liquid state.<sup>52</sup>

Reheating to  $-20\text{ }^{\circ}\text{C}$  at a heating rate of  $40\text{ }^{\circ}\text{C}/\text{min}$  causes the  $\alpha$ -helix band at  $1270\text{ cm}^{-1}$  to diminish by about 20%, now the protein shows the typical  $\beta$ -sheet secondary structure at  $1243\text{ cm}^{-1}$  (see Fig. 3, red trace and dashed vertical lines). Also, the phenylalanine band at  $1008\text{ cm}^{-1}$  is now much less intense (see dashed vertical line). Generally speaking, structural changes can be only estimated roughly by comparing intensities within the same spectra. In this work results have to be seen as a qualitative comparison rather than quantitative results. The tyrosine ratio, calculated by the band intensity ratio  $(856\text{ cm}^{-1})/(830\text{ cm}^{-1})$ , of 1.2 at  $-20\text{ }^{\circ}\text{C}$  indicates a relative increase of exposed tyrosine residues (see Fig. 3, grey box and dashed vertical lines).

Raman spectra after cooling and reheating, both at  $20\text{ }^{\circ}\text{C}/\text{min}$ , at various temperatures in the thawing step are shown in Fig. 4. In the Amide III region ( $1200\text{ cm}^{-1}$ – $1280\text{ cm}^{-1}$ ) the spectra at  $-80\text{ }^{\circ}\text{C}$  and  $-60\text{ }^{\circ}\text{C}$  show three features. The highest intensity is seen at  $1238\text{ cm}^{-1}$ , followed by  $1253\text{ cm}^{-1}$  and  $1268\text{ cm}^{-1}$ , representing  $\beta$ -sheet, random coil and  $\alpha$ -helix in order of intensities (see Fig. 4A). At  $-50\text{ }^{\circ}\text{C}$  the secondary structure of the protein changes: the random coil band at  $1253\text{ cm}^{-1}$  diminishes, and the  $1268\text{ cm}^{-1}$  band assigned to  $\alpha$ -helix becomes more prominent, surpassing the previously most intense  $\beta$ -sheet band. Upon further heating to  $-40\text{ }^{\circ}\text{C}$  and  $-30\text{ }^{\circ}\text{C}$  the band assigned to  $\beta$ -sheet at  $1238\text{ cm}^{-1}$  becomes more intense again, whereas intensities of random coil and  $\alpha$ -helix bands decrease.

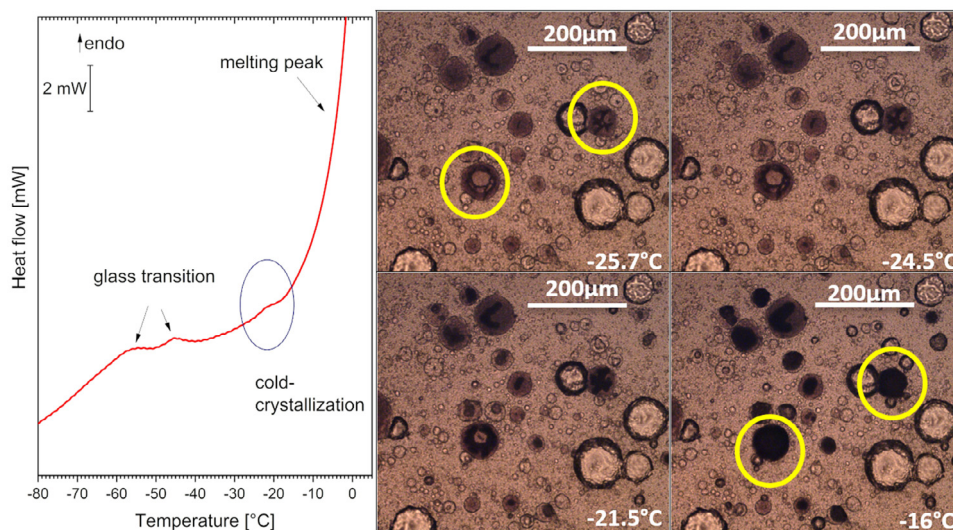


**Figure 2.** Differential Scanning Calorimetry thermogram recorded at a heating rate of  $60\text{ }^{\circ}\text{C}/\text{min}$  (left) and microscopy images (right) of droplets containing mab formulation 1 in emulsion during heating.<sup>26</sup>

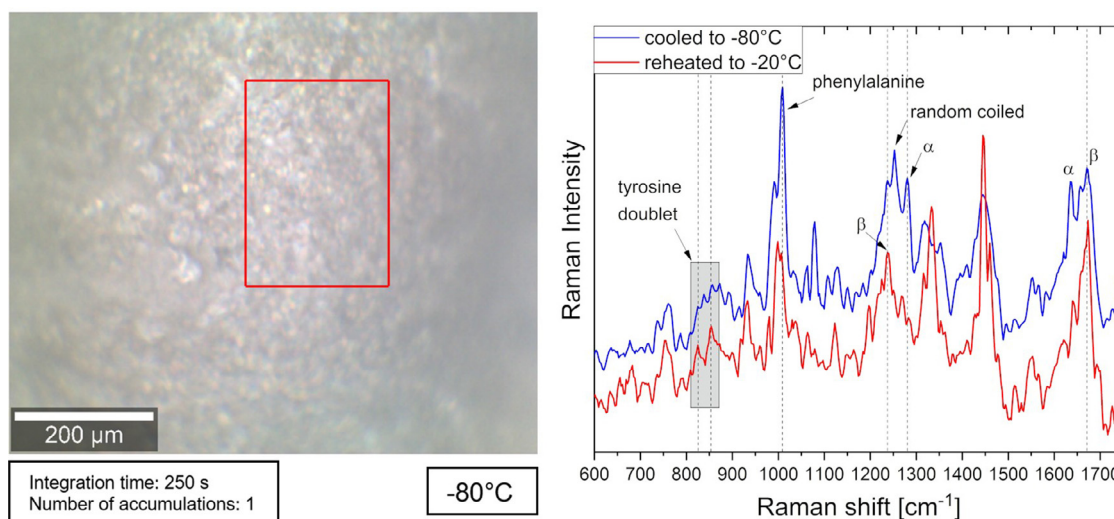


**Figure 3.** (left) Microscope image of mab formulation recorded at  $-80^{\circ}\text{C}$ . The red square indicates the position for the large area scan. (right) Raman spectra recorded at  $-80^{\circ}\text{C}$  after cooling at  $40^{\circ}\text{C}/\text{min}$  (blue trace) and after reheating to  $-20^{\circ}\text{C}$  at  $40^{\circ}\text{C}/\text{min}$  (red trace). Spectra are averages of 16 single spectra obtained by scanning a selected area (red square in left image) within the droplet.

In the Amide I region ( $1620\text{ cm}^{-1}$ – $1700\text{ cm}^{-1}$ ) a splitting of the  $\beta$ -sheet band at around  $1670\text{ cm}^{-1}$  at  $-80^{\circ}\text{C}$ ,  $-60^{\circ}\text{C}$  and  $-40^{\circ}\text{C}$  is observed (see Fig. 4B, vertical lines labelled  $\beta$  and  $\beta'$ ). Interestingly, this splitting is absent at  $-50^{\circ}\text{C}$  whereas the intensity of the  $\alpha$ -helix band at  $1640\text{ cm}^{-1}$  increases (see Fig. 4B, vertical lines labelled  $\alpha$ ) simultaneously with the disappearance of the splitting. The most intense band at  $-50^{\circ}\text{C}$  is located at  $1673\text{ cm}^{-1}$ , which indicates  $\beta$ -sheet structures. Upon heating to  $-40^{\circ}\text{C}$  the  $\alpha$ -helix band decreases in intensity and the  $\beta$ -sheet band splits in the same way seen at  $-60^{\circ}\text{C}$ , one maximum at  $1665\text{ cm}^{-1}$  and one at  $1673\text{ cm}^{-1}$ . On further heating to  $-30^{\circ}\text{C}$  the  $\alpha$ -helix band disappears and the split band merges with a maximum at  $1665\text{ cm}^{-1}$ . It stays there up to  $0^{\circ}\text{C}$  (data not shown). The corresponding tyrosine ratios are shown in Fig. 4C. At  $-80^{\circ}\text{C}$  the tyrosine intensity ratio is 1, both bands in the grey shaded area are equally intense. The ratio is displayed also numerically in Fig. 4C (value mentioned at the right end of each curve). After heating to  $-60^{\circ}\text{C}$  the tyrosine ratio increases to 1.7 (spectra is close to limit-of-detection and there shows a very high single-to-

noise-ratio). Upon further heating the protein shows again a tyrosine ratio of 1 concluding with a final ratio of 1.2 at  $-30^{\circ}\text{C}$ .

#### Structural Changes Upon Thawing of The Three Different Mab Formulations

Raman spectra at various temperatures mab formulation 2 and mab formulation 3 after cooling to  $-80^{\circ}\text{C}$  at  $20^{\circ}\text{C}/\text{min}$  and stepwise reheating to  $-20^{\circ}\text{C}$  are shown in Fig. 5 and Fig. 6, respectively.

In mab formulation 2 spectra in the Amide III region ( $1200\text{ cm}^{-1}$ – $1280\text{ cm}^{-1}$ ) recorded at  $-80^{\circ}\text{C}$  show a  $\beta$ -sheet structure with a vague  $\alpha$ -helix (see Fig. 5A). Upon heating a random coil structure becomes more prominent, especially at  $-60^{\circ}\text{C}$ , and can be seen in spectra up to  $-20^{\circ}\text{C}$ . In the Amide I region ( $1620\text{ cm}^{-1}$ – $1700\text{ cm}^{-1}$ ) most of the spectra show a parallel  $\beta$ -sheet with a small contribution of  $\alpha$ -helix at  $1645\text{ cm}^{-1}$  (see Fig. 5B). Only at the highest temperature of  $-20^{\circ}\text{C}$  the parallel  $\beta$ -sheet shifts to an antiparallel  $\beta$ -sheet structure. The tyrosine ratio starts at 1.2 for  $-80^{\circ}\text{C}$  (see Fig. 5C). Upon heating the

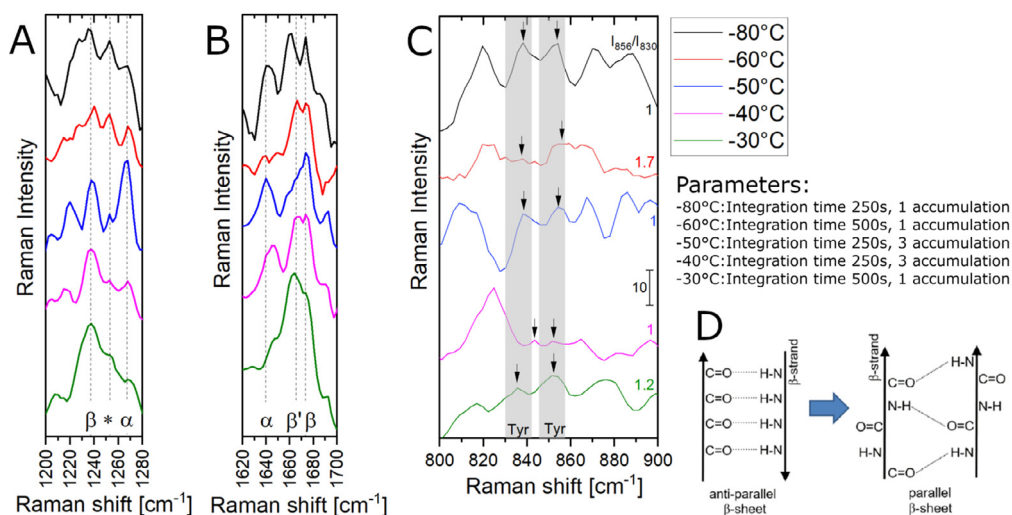


**Figure 4.** Raman spectra of mab formulation 1 (A) in the Amide III region, (B) Amide I region and (C) tyrosine doublet region after cooling to  $-80^{\circ}\text{C}$  at  $20^{\circ}\text{C}/\text{min}$  and stepwise reheating to  $-30^{\circ}\text{C}$  at a rate of  $20^{\circ}\text{C}/\text{min}$ .  $\beta$  and  $\beta'$  represent anti-parallel and parallel  $\beta$ -sheet, respectively,  $\alpha$  indicates the band assigned to  $\alpha$ -helix and \* indicates the position of random coil marker band. (D) Schematic depiction of anti-parallel and parallel  $\beta$ -sheets.

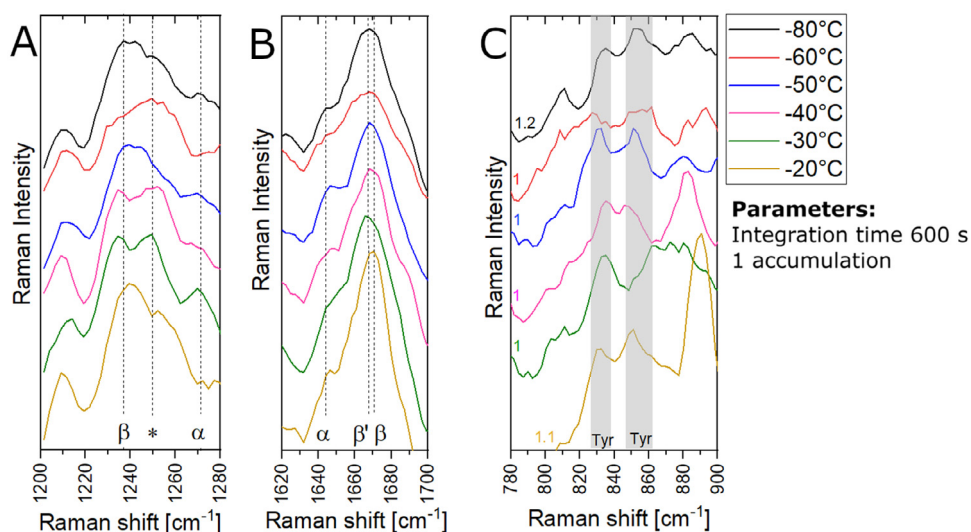


**Figure 5.** Raman spectra of mab formulation 2 (A) in the Amide III region, (B) Amide I region and (C) tyrosine doublet region after cooling to  $-80^{\circ}\text{C}$  at  $20^{\circ}\text{C}/\text{min}$  and stepwise reheating to  $-20^{\circ}\text{C}$  at a rate of  $20^{\circ}\text{C}/\text{min}$ .  $\beta$  and  $\beta'$  represent anti-parallel and parallel  $\beta$ -sheet, respectively,  $\alpha$  indicates the band assigned to  $\alpha$ -helix and \* indicates the position of the bands assigned to random coil. Locations of marker bands for  $\alpha$ ,  $\beta$ ,  $\beta'$  and random coil are indicated by vertical dashed lines.

ratio stays at 1 for  $-60^{\circ}\text{C}$ ,  $-50^{\circ}\text{C}$ ,  $-40^{\circ}\text{C}$  and  $-30^{\circ}\text{C}$ . At  $-20^{\circ}\text{C}$  a small increase of tyrosine ratio to 1.1 can be detected.

Raman spectra of mab formulation 3 containing mannitol feature  $\beta$ -sheet structures at  $-80^{\circ}\text{C}$ . This can be seen in the Amide III region ( $1200\text{ cm}^{-1}$ – $1280\text{ cm}^{-1}$ ) at  $1240\text{ cm}^{-1}$  (see Fig. 6A). Upon heating to  $-20^{\circ}\text{C}$  the  $\beta$ -sheet structure first changes to random coil and then reverts to  $\beta$ -sheet. At  $-50^{\circ}\text{C}$  random coil and a small band assigned to  $\alpha$ -helix can be seen. An increase of  $\alpha$ -helix structures can be also seen in the corresponding Amide I region at  $1640\text{ cm}^{-1}$  ( $1620\text{ cm}^{-1}$ – $1700\text{ cm}^{-1}$ ) (see Fig. 6B). The signatures for  $\alpha$ -helix fade away upon heating to higher temperatures. At  $-20^{\circ}\text{C}$  the  $\beta$ -sheet structure has developed again. This implies that the mab solution is not stable near  $-50^{\circ}\text{C}$ , but starts to be mobile in the freeze-concentrated solution that slowly get less viscous upon heating, ultimately leading to transformations of the mab upon heating beyond the glass transition.

Similar observations can be made on the basis of the tyrosine ratio, where changes are observed even at  $-60^{\circ}\text{C}$ . The tyrosine ratio

at  $-80^{\circ}\text{C}$  shows a starting value of 1.6 (see Fig. 6C). Upon heating the ratio decreases to 1 at  $-60^{\circ}\text{C}$  and at  $-50^{\circ}\text{C}$ ; increases again to 1.3 at  $-40^{\circ}\text{C}$  and  $-30^{\circ}\text{C}$ . At a temperature of  $-20^{\circ}\text{C}$  the tyrosine ratio displays a value of 1. This again demonstrates that the mab solution is far from immobile and stable upon heating, especially in the temperature range between  $-60^{\circ}\text{C}$  and  $-20^{\circ}\text{C}$ . In this temperature range the fully frozen solution first experiences decrease of viscosity within the freeze-concentrated solution, where the solution probably forms a network of veins threading through the ice crystals. Upon continued heating this network of veins may experience cold-crystallization of veins, again causing changes in concentration and favoring changes in the protein, especially aggregation. Furthermore, a second type of freeze-concentrated solution that is homogeneously distributed over all the ice and interweaved between needles may also be present. The two types of freeze-concentrated solution form through macro- and microcryoconcentration, respectively. This second solution of different concentration experiences its glass transition at a

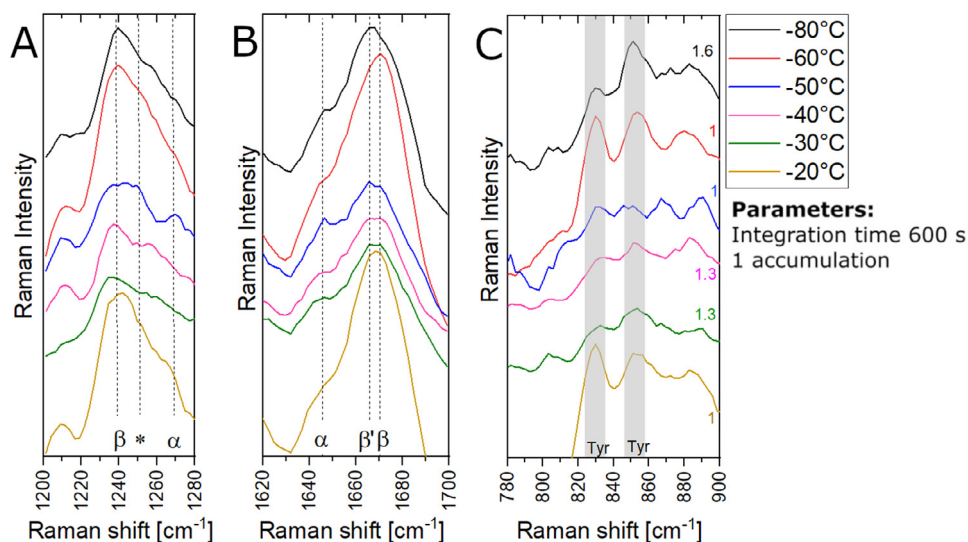


**Figure 6.** Raman spectra of mab formulation 3 (A) in the Amide III region, (B) Amide I region and (C) tyrosine doublet region after cooling to  $-80^{\circ}\text{C}$  at  $20^{\circ}\text{C}/\text{min}$  and stepwise reheating to  $-20^{\circ}\text{C}$  at a rate of  $20^{\circ}\text{C}/\text{min}$ .  $\beta$  and  $\beta'$  represent anti-parallel and parallel  $\beta$ -sheet, respectively,  $\alpha$  indicates the band assigned to  $\alpha$ -helix and \* indicates the position of the bands assigned to random coil.

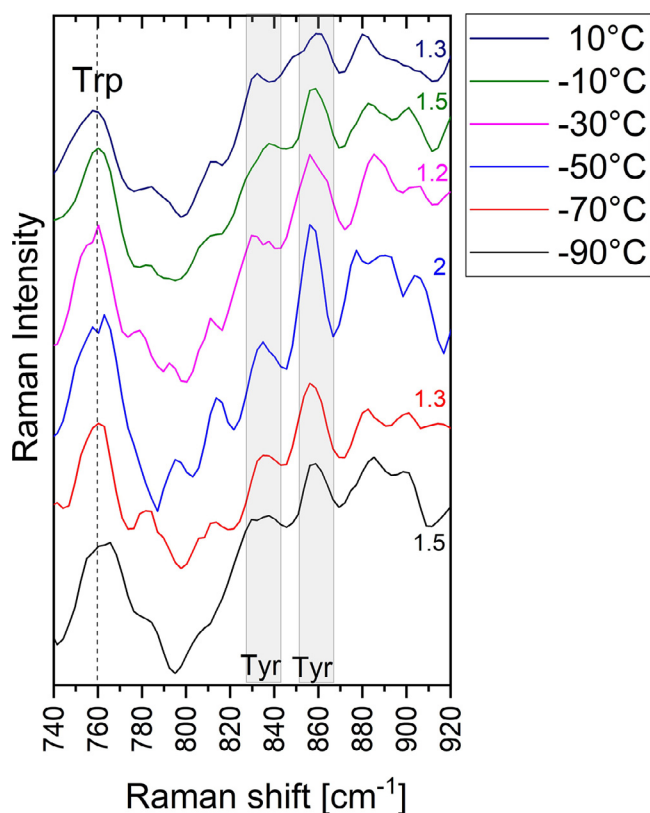


**Figure 7.** Raman spectra of mAb formulation 1 containing a higher number of aggregates during heating from  $-90^{\circ}\text{C}$  to  $10^{\circ}\text{C}$  in  $20^{\circ}\text{C}$ -steps (each spectrum was recorded with an integration time of 200 seconds/3 accumulations).

somewhat different temperature, so that mAb located in the space between ice crystals rather than in the vein network experiences its changes at somewhat different temperature. In the end, this implies that the changes of the mAb structure, including change of secondary structure and aggregation, do not take place at a specific temperature, but in a broad range that we here see between  $-60^{\circ}\text{C}$  and  $-20^{\circ}\text{C}$ .

#### Validation of the Use of Tyrosine Intensity Ratio $I_{856}/I_{830}$ as a Marker of Mab Aggregation

The tyrosine ratio in the mAb formulation 1 that was on purpose aggregated by heavy shaking at higher temperatures (see Experimental) confirms its diagnostic quality. The sample cooled directly to  $-90^{\circ}\text{C}$  was heated in  $20^{\circ}\text{C}$  steps up to  $10^{\circ}\text{C}$  and features tyrosine ratios between 1.2 and 2, higher than the range of 1 to 1.7 in the sample that was frozen without shaking (see Fig. 7).

## Discussion

### Influence of Cooling Rate on the Secondary Structure of Mab Formulation 1

Cooling to  $-80^{\circ}\text{C}$  at rates of  $40^{\circ}\text{C}/\text{min}$  results in structural changes within the mAb formulation 1 (see Fig. 3). Upon cooling the native secondary structure of mAb changes from  $\beta$ -sheet in the liquid state<sup>52</sup> to random coil and  $\alpha$ -helix as evidenced by an increase of the Raman bands at  $1251\text{ cm}^{-1}$  for random coil and at  $1270\text{ cm}^{-1}$  and  $1635\text{ cm}^{-1}$  for  $\alpha$ -helix (see Fig. 3). By heating to  $-20^{\circ}\text{C}$  the mAb represents a native protein structure, an antiparallel  $\beta$ -sheet structure. The observation of native structures could be caused by the

devitrification of freeze-concentrated solution at  $-20^{\circ}\text{C}$  (above glass transition temperature; see Fig. 2) which may give the protein the mobility necessary to rearrange.

Additionally, the Raman spectrum at  $-80^{\circ}\text{C}$  shows an increase of the intensity of the phenylalanine band at  $1008\text{ cm}^{-1}$ . This indicates pre-aggregation according to ref.<sup>42</sup> An increase of Raman intensity at  $1008\text{ cm}^{-1}$  can be explained by the mAb unfolding aromatic side chains (in this case phenylalanine) which become more exposed to the buffer solution.<sup>53</sup> In previous studies the phenylalanine band at around  $1000\text{ cm}^{-1}$  is said to be useful marker for storage stability.<sup>42</sup>

In our experiments, after heating to  $-20^{\circ}\text{C}$  at  $40^{\circ}\text{C}/\text{min}$  the Raman spectra show a tyrosine ratio of 1.2. In spite of the very fast heating, much faster than typically employed in pharmaceutical industry, the time is still sufficient to induce severe changes of the mAb upon thawing. As alluded to above, in the temperature range between  $-60^{\circ}\text{C}$  and  $-20^{\circ}\text{C}$  two types of fully frozen freeze-concentrated solutions slowly turn into the liquids, where also cold-crystallization of the ice in these spots might result in increases of local mAb concentration – thus favoring aggregation. Our results support the statement that an increase of the phenylalanine band can be used as an indicator for pre-aggregation.

These changes very much depend on the time available for them to occur. Thus, the behavior at a cooling and heating rate of  $20^{\circ}\text{C}/\text{min}$  is quite different. Hereby, only changes of secondary structure in the Amide I and Amide III region are observed in the range up to  $-30^{\circ}\text{C}$ . Slight changes in the tyrosine intensity ratio could be noticed during heating, the ratio in most spectra is calculated to be 1, with the only significant exception at  $-60^{\circ}\text{C}$  where the ratio increases to 1.4. Compared to the data obtained from cooling mAb formulation 1 at  $40^{\circ}\text{C}/\text{min}$ , this freezing protocol seems to have less impact on the secondary structure. The Amide III region in Fig. 4 shows three bands at  $1238\text{ cm}^{-1}$ ,  $1253\text{ cm}^{-1}$  and  $1268\text{ cm}^{-1}$ , assigned to  $\beta$ -sheet, random coil and  $\alpha$ -helix. All three bands are visible in spectra recorded at  $-80^{\circ}\text{C}$  and  $-60^{\circ}\text{C}$ , in order of decreasing intensity. At  $-50^{\circ}\text{C}$  a significant structural rearrangement of mAb occurs whereas the conformation of an  $\alpha$ -helix becomes most dominant (see Fig. 4).

Upon further heating the band assigned to the  $\alpha$ -helix structure decreases and the protein presents itself in its native secondary structure, the  $\beta$ -sheet. One of the most prominent changes in the spectra is the observed splitting of the  $\beta$ -sheet band in the Amide I region. This feature appears already in the first spectra recorded at  $-80^{\circ}\text{C}$  after cooling at  $20^{\circ}\text{C}/\text{min}$ . These two bands, one at  $1665\text{ cm}^{-1}$  and one at  $1673\text{ cm}^{-1}$ , are assigned to parallel and antiparallel  $\beta$ -sheets. Upon heating the splitting indicates that both structures, parallel and antiparallel  $\beta$ -sheet, are present until reaching  $-50^{\circ}\text{C}$ , where the mAb structure is detected in its antiparallel  $\beta$ -sheet conformation (see Fig. 4). At  $-40^{\circ}\text{C}$  the protein starts rearranging to  $\beta$ -sheets again, indicating by the splitting of the band in the Amide I region. At  $-30^{\circ}\text{C}$  the parallel  $\beta$ -sheet conformation dominates. It is expected that the mAb secondary structure returns back to the native conformation (antiparallel  $\beta$ -sheets) upon further heating.

In other words, the tyrosine ratio and the Raman marker bands suggest a transition at  $-50^{\circ}\text{C}$ . According to the calorimetry data this transition already takes place near the lower-lying glass transition temperature. Starting from the lower-lying glass transition then severe changes take place upon heating, where the heating rate and thus the time available for the changes to occur determine the dominant processes. The mAb located in the veins and the mAb located between interweaved ice crystals may change, and additionally cold-crystallization may cause changes of mAb concentration in both regions. Ultimately, this leads to a complex set of changes in the mAb that very much depends on heating rate in the range between  $-60^{\circ}$  and  $-20^{\circ}\text{C}$ . At lower temperatures the fully frozen solution is stable, at higher temperatures the melting of the solution progresses according to thermodynamics. In addition to the heating rate also the

**Table 3**  
Summary of secondary structural changes of mab formulations obtained from the Amide III and Amide I region of Raman spectra of Figs. 4–6. Measurement series started after cooling to –80 °C at 20 °C/min and heating stepwise to –60 °C, –50 °C, –40 °C, –30 °C and –20 °C at 20 °C/min. The + (plus) between two secondary characteristics indicate that both structures are having the same Raman intensity in the spectrum.

T	Mab formulation 1			Mab formulation 2			Mab formulation 3		
	Amide III	Amide I	Tyr/Tyr	Amide III	Amide I	Tyr/Tyr	Amide III	Amide I	Tyr/Tyr
<b>-80 °C</b>	$\beta$ -sheet, random coil, $\alpha$ -helix	Split $\beta$ -sheet, small $\alpha$ -helix	1	$\beta$ -sheet, small $\alpha$ -helix	Parallel $\beta$ -sheet	1.2	$\beta$ -sheet	Parallel $\beta$ -sheet	1.6
<b>-60 °C</b>	$\beta$ -sheet	Split $\beta$ -sheet, small $\alpha$ -helix	1.7	random coil	Parallel $\beta$ -sheet	1	$\beta$ -sheet	Anti-Parallel $\beta$ -sheet	1
<b>-50 °C</b>	High $\alpha$ -helix, $\beta$ -sheet, small random coil	Anti-parallel $\beta$ -sheet, $\alpha$ -helix	1	$\beta$ -sheet, small $\alpha$ -helix	Parallel $\beta$ -sheet, small $\alpha$ -helix	1	$\beta$ -sheet + random coil, small $\alpha$ -helix	Split $\beta$ -sheet, small $\alpha$ -helix	1
<b>-40 °C</b>	$\beta$ -sheet, random coil, $\alpha$ -helix	Split $\beta$ , $\alpha$ -helix	1	Split $\beta$ -sheet + random coil	Anti-parallel $\beta$ -sheet, small $\alpha$ -helix	1	$\beta$ -sheet, small random coil	Parallel $\beta$ -sheet	1.3
<b>-30 °C</b>	$\beta$ -sheet	Parallel $\beta$ -sheet	1.2	Split $\beta$ -sheet + random coil	Parallel $\beta$ -sheet	1	$\beta$ -sheet	Parallel $\beta$ -sheet, small $\alpha$ -helix	1.3
<b>-20 °C</b>	-	-	-	Split $\beta$ -sheet, small random coil	Anti-parallel $\beta$	1.1	$\beta$ -sheet	Anti-parallel $\beta$ -sheet	1

cryoprotectants in the solution play a major role, as summarized in the next section.

### Structural Changes Upon Thawing of the Three Different Mab Formulations

Qualitative changes in the Amide III and Amide I regions upon thawing, are summarized in Table 3. For direct comparison of intensities in spectra see Figs. 4–6. Of all three formulations mab formulation 3 containing mannitol shows the least secondary structural changes of IgG1. Most notably, fewer  $\alpha$ -helices and random coil structures are observed in mab formulation 3 (see Fig. 6, A and B).

For all mab formulations the majority of structural changes of protein in formulation occurs between –60 °C and –40 °C. At this temperature range two  $T_g$ 's, one at –58 °C and one at –48 °C respectively, have been detected for mab formulation 1 by DSC (see Fig. 2). The change of secondary structure at this temperature region is likely related to the increase of mobility of the protein that is triggered by the decrease of viscosity above  $T_g$ . Furthermore, the change of secondary structure at around –50 °C is in accordance with what has been described in literature: hydrated protein shows some kind of dynamic transition at 220 K.<sup>54–61</sup> This dynamic transition at around –50 °C can also be detected by DSC as a glass transition in the thermogram (see Fig. 2). At –20 °C most of the mab formulations appear in the native conformation with a tyrosine ratio of approx. 1.

### Validation of the Use of Tyrosine Intensity Ratio $I_{856}/I_{830}$ as a Marker of Mab Aggregation

Raman measurements of mab formulation with a high number of aggregates validate the use of the tyrosine intensity ratio  $I_{856}/I_{830}$  as an indicator for aggregation. The ratio  $I_{856}/I_{830}$  of spectra recorded at –90 °C, –70 °C, –50 °C, –30 °C, –10 °C and 10 °C are 1.5, 1.3, 2, 1.2, 1.5 and 1.3, respectively, in the order of increasing temperature. In the liquid state (at 10 °C) a tyrosine intensity ratio of 1.3 remains. The detection of the highest tyrosine intensity ratio at –50 °C may be traced back to the dynamic transition associated with the possible rearrangement of the antibody (tyrosine residues become more exposed to the buffer solution) in the freeze concentrated solution within the droplet.

A decrease of the ratio  $I_{856}/I_{830}$  is an indication for tertiary structural changes of protein in which tyrosine residues as donors are more strongly hydrogen bonded to a negative-charge receptor, e.g., a carboxylate ion.<sup>37</sup>

Our results demonstrate that the tyrosine intensity ratio  $I_{856}/I_{830}$  in Raman spectra is an excellent marker both for tertiary structural changes and aggregates.

## Conclusion

Raman spectroscopy is shown here to be a highly versatile for assessing protein structures in the frozen state. Specifically, the Amide I-III bands in the fingerprint region are demonstrated to be highly useful to follow secondary and tertiary structure changes in an IgG1 antibody's.

Hereby, changes of secondary structure, including  $\alpha$ -helix,  $\beta$ -sheet and random coil, and change of tertiary structure, can be detected in the frozen solution upon thawing. The latter is accomplished by evaluation of the ratio of tyrosine bands at 856  $\text{cm}^{-1}$  and 830  $\text{cm}^{-1}$ , as a marker for mab aggregation.

A cooling rate of 40 °C/min results in an increased presence of random coil and  $\alpha$  -helices within formulation 1 at –80 °C. Reduced cooling rate to 20 °C/min results in fewer secondary structural changes at –80 °C.

Upon heating to –20 °C the protein's secondary structure undergoes changes in all mab formulation.

These secondary structural changes can be backtraced to the trespassing of up to two glass transition temperatures of two different types of freeze-concentrated solution, where the local mab concentrations differ due to macro- and microcryoconcentration upon freezing and due to devitrification of these freeze-concentrated solutions at different temperatures in the range between  $-60^{\circ}\text{C}$  and  $-20^{\circ}\text{C}$ . Above both  $T_g$ s the protein gains mobility, leading to exposure of certain amino acid residues at the proteins' surface to the solvent (e.g., tyrosine) and/or relaxation (from parallel- to anti-parallel  $\beta$ -sheet). The interplay between the different types of solution, including cold-crystallization, is very complex depending very much on details such as initial mab concentration, heating rate and type of cryoprotectant. By comparing three formulations of the same mab we demonstrate that the mab formulation containing the least protein shows the most structural changes, whereas an increase of mab content leads to less changes upon heating indicating higher stability.

An increase of protein concentration and the addition of mannitol results in even fewer changes of secondary structure. That is, we recommend mannitol formulations and slow cooling for the freeze-thaw cycle of IgG1 solutions to avoid protein aggregation. Even more importantly, our work demonstrates that Raman spectroscopy is a powerful method for determining structural changes of protein and aggregation in the frozen state.

### Declaration of Interests

The authors declare that they have no known competing financial interests or personal relationships that could have appeared to influence the work reported in this paper.

### Acknowledgements

We are grateful to Sandoz GmbH and Novartis Pharma AG for financial support.

### Supplementary Materials

Supplementary material associated with this article can be found in the online version at doi:[10.1016/j.xphs.2022.10.015](https://doi.org/10.1016/j.xphs.2022.10.015).

### References

- Kolhe P, Badkar A. Protein and solute distribution in drug substance containers during frozen storage and post-thawing: A tool to understand and define freezing-thawing parameters in biotechnology process development. *Biotechnol Prog*. 2011;27(2):494–504.
- Strambini GB, Gabellieri E. Proteins in frozen solutions: Evidence of ice-induced partial unfolding. *Biophys J*. 1996;70(2):971–976.
- Hsu CC, Nguyen HM, Yeung DA, et al. Surface denaturation at solid-void interface – a possible pathway by which opalescent particulates form during the storage of lyophilized tissue-type plasminogen-activator at high-temperatures. *Pharm Res*. 1995;12(1):69–77.
- Rosenberg AS. Effects of protein aggregates: An immunologic perspective. *AAPS J*. 2006;8(3):E501–E507.
- Hermeling S, Crommelin DJA, Schellekens H, Jiskoot W. Structure-immunogenicity relationships of therapeutic proteins. *Pharm Res*. 2004;21(6):897–903.
- Carpenter JF, Randolph TW, Jiskoot W, et al. Overlooking subvisible particles in therapeutic protein products: gaps that may compromise product quality. *J Pharm Sci*. 2009;98(4):1201–1205.
- Mahler HC, Friess W, Gauschopf U, Kiese S. Protein aggregation: pathways, induction factors and analysis. *J Pharm Sci*. 2009;98(9):2909–2934.
- Hauptmann A, Hoelzl G, Loerting T. Distribution of protein content and number of aggregates in monoclonal antibody formulation after large-scale freezing. *AAPS PharmSciTech*. 2019;20(2):72.
- Kueltzo LA, Wang W, Randolph TW, Carpenter JF. Effects of solution conditions, processing parameters, and container materials on aggregation of a monoclonal antibody during freeze-thawing. *J Pharm Sci*. 2008;97(5):1801–1812.
- Hillgren A, Lindgren J, Alden M. Protection mechanism of Tween 80 during freeze-thawing of a model protein, LDH. *Int J Pharm*. 2002;237(1–2):57–69.
- Kreilgaard L, Jones LS, Randolph TW, et al. Effect of Tween 20 on freeze-thawing and agitation-induced aggregation of recombinant, human factor XIII. *J Pharm Sci*. 1998;87(12):1597–1603.
- Schenz TW. Glass transitions and product stability – an overview. *Food Hydrocoll*. 1995;9(4):307–315.
- Miller MA, Rodrigues MA, Glass MA, Singh SK, Johnston KP, Maynard JA. Frozen-state storage stability of a monoclonal antibody: aggregation is impacted by freezing rate and solute distribution. *J Pharm Sci*. 2013;102(4):1194–1208.
- Barnard JG, Singh S, Randolph TW, Carpenter JF. Subvisible particle counting provides a sensitive method of detecting and quantifying aggregation of monoclonal antibody caused by freeze-thawing: insights into the roles of particles in the protein aggregation pathway. *J Pharm Sci*. 2011;100(2):492–503.
- Sundaramurthi P, Suryanarayanan R. The effect of crystallizing and non-crystallizing cosolutes on succinate buffer crystallization and the consequent pH shift in frozen solutions. *Pharm Res*. 2011;28(2):374–385.
- Bhatnagar BS, Pikal MJ, Bogner RH. Study of the individual contributions of ice formation and freeze-concentration on isothermal stability of lactate dehydrogenase during freezing. *J Pharm Sci*. 2008;97(2):798–814.
- Levine H, Slade L. Thermomechanical properties of small-carbohydrate-water glasses and 'rubbers'. Kinetically metastable systems at sub-zero temperatures. *J Chem Soc, Faraday Trans.*. 1988;84(8):2619–2633.
- Hauptmann A, Hoelzl G, Loerting T. Optical cryomicroscopy and differential scanning calorimetry of buffer solutions containing cryoprotectants. *Eur J Pharm Biopharm*. 2021;163:127–140.
- Jena S, Horn J, Suryanarayanan R, Friess W, Aksan A. Effects of excipient interactions on the state of the freeze-concentrate and protein stability. *Pharm Res*. 2017;34(2):462–478.
- Mezhebovsky T, Routhier E, Sass P, Shahrokh Z. Enabling freeze-thaw stability of PBS-based formulations of a monoclonal antibody Part II: Long-term frozen storage. *Biopharm Int*. 2016;29(9):38–47.
- Mezhebovsky T, Routhier E, Sass P, Shahrokh Z. Enabling freeze-thaw stability of PBS-based formulations of a monoclonal antibody Part I: Freeze-thaw stress testing. *Biopharm Int*. 2016;29(8):33–39.
- Chavez BK, Agarabi CD, Read EK, Boyne II MT, Khan MA, Brorson KA. Improved stability of a model IgG3 by DoE-based evaluation of buffer formulations. *BioMed Res Int*. 2016.
- Liu L, Braun LJ, Wang W, Randolph TW, Carpenter JF. Freezing-induced perturbation of tertiary structure of a monoclonal antibody. *J Pharm Sci*. 2014;103(7):1979–1986.
- Infrared Spectroscopy of n-Methylacetamide in Solid Parahydrogen [Internet]*. Ohio State University; 2006. [cited 15th Aug 2018]. Available from: <https://kb.osu.edu>.
- Foggia MD, Taddei P, Torreggiani A, Dettin M, Tinti A. Self-assembling peptides for biomedical applications: IR and Raman spectroscopies for the study of secondary structure. *J Proteome Res*. 2012;2(3):231–272.
- Hauptmann A. Characterization of Aqueous Drug Substance During Freezing and Thawing. University Innsbruck; 2019. Doctoral Thesis.
- Wen Z-Q. Raman spectroscopy of protein pharmaceuticals. *J Pharm Sci*. 2014;103(8):2590.
- Vedantham G, Sparks HG, Sane SU, Tzannis S, Przybycien TM. A holistic approach for protein secondary structure estimation from infrared spectra in H(2)O solutions. *Anal Biochem*. 2000;285(1):33–49.
- Peters J, Luczak A, Ganesh V, Park E, Kalyanaraman R. Protein secondary structure determination using drop coat deposition confocal Raman spectroscopy. *Spectroscopy*. 2016;31(10):31–39.
- David C, Foley S, Mavon C, Enescu M. Reductive unfolding of serum albumins uncovered by Raman spectroscopy. *Biopolymers*. 2008;89(7):623–634.
- Pelton JT, McLean LR. Spectroscopic methods for analysis of protein secondary structure. *Anal Biochem*. 2000;277(2):167–176.
- Rygula A, Majzner KM, Marzec K, Kaczor A, Pilarczyk M, Baranska M. Raman spectroscopy of proteins: a review. *J Raman Spectrosc*. 2013;44(8):1061–1076.
- Schwegman JJ, Carpenter JF, Nail SL. Evidence of partial unfolding of proteins at the ice/freeze-concentrate interface by infrared microscopy. *J Pharm Sci*. 2009;98(9):3239–3246.
- Maiti NC, Apetri MM, Zagorski MG, Carey PR, Anderson VE. Raman spectroscopic characterization of secondary structure in natively unfolded proteins: alpha-synuclein. *J Am Chem Soc*. 2004;126(8):2399–2408.
- Apetri MM, Maiti NC, Zagorski MG, Carey PR, Anderson VE. Secondary structure of alpha-synuclein oligomers: characterization by raman and atomic force microscopy. *J Mol Biol*. 2006;355(1):63–71.
- Barnett GV, Qi W, Amin S, et al. Structural changes and aggregation mechanisms for anti-streptavidin IgG1 at elevated concentration. *J Phys Chem B*. 2015;119(49):15150–15163.
- Zhou C, Qi W, Lewis EN, Carpenter JF. Concomitant Raman spectroscopy and dynamic light scattering for characterization of therapeutic proteins at high concentrations. *Anal Biochem*. 2015;472:7–20.
- Baker AE, Mantz AR, Chiu ML. Raman spectroscopy characterization of antibody phases in serum. *mAbs*. 2014;6(6):1509–1517.
- Smith LJ, Fiebig KM, Schwalbe H, Dobson CM. The concept of a random coil: residual structure in peptides and denatured proteins. *Fold Des*. 1996;1(5):R95–R106.
- David C, Foley S, Enescu M. Protein S-S bridge reduction: a Raman and computational study of lysozyme interaction with TCEP. *Phys Chem Chem Phys*. 2009;11(14):2532–2542.

41. Wei F, Zhang D, Halas NJ, Hartgerink JD. Aromatic amino acids providing characteristic motifs in the Raman and SERS spectroscopy of peptides. *J Phys Chem B*. 2008;112(30):9158–9164.
42. Ota C, Noguchi S, Nagatoishi S, Tsumoto K. Assessment of the protein–protein interactions in a highly concentrated antibody solution by using Raman spectroscopy. *Pharm Res*. 2016;33(4):956–969.
43. Kengne-Momo RP, Daniel P, Lagarde F, et al. Protein interactions investigated by the Raman spectroscopy for biosensor applications. *Int J Spectrosc*. 2012. 2012.
44. Podstawka E, Sikorska E, Proniewicz LM, Lammek B. Raman and surface-enhanced Raman spectroscopy investigation of vasopressin analogues containing 1-amino-cyclohexane-1-carboxylic acid residue. *Biopolymers*. 2006;83(2):193–203.
45. Sugeta H, Go A, Miyazawa T. S–S and C–S stretching vibrations and molecular conformations of dialkyl disulfides and cystine. *Chem Lett*. 1972;1(1):83–86.
46. Siamwiza MN, Lord RC, Chen MC, et al. Interpretation of the doublet at 850 and 830 cm<sup>-1</sup> in the Raman spectra of tyrosyl residues in proteins and certain model compounds. *Biochemistry*. 1975;14(22):4870–4876.
47. Ota C, Noguchi S, Tsumoto K. The molecular interaction of a protein in highly concentrated solution investigated by Raman spectroscopy. *Biopolymers*. 2015;103(4):237–246.
48. Chari R, Jerath K, Badkar AV, Kalonia DS. Long- and short-range electrostatic interactions affect the rheology of highly concentrated antibody solutions. *Pharm Res*. 2009;26(12):2607–2618.
49. Wong H-W, Choi S-M, Phillips DL, Ma C-Y. Raman spectroscopic study of deamidated food proteins. *Food Chem*. 2009;113(2):363–370.
50. Li-Chan ECY. The applications of Raman spectroscopy in food science. *Trends Food Sci Technol*. 1996;7(11):361–370.
51. Hauptmann A, Handle KF, Baloh P, Grothe H, Loerting T. Does the emulsification procedure influence freezing and thawing of aqueous droplets? *J Chem Phys*. 2016;145(21): 211923.
52. Wen Z-Q. Raman spectroscopy of protein pharmaceuticals. *J Pharm Sci*. 2007;96(11):2861–2878.
53. Abbas SA, Gaspar G, Sharma VK, Patapoff TW, Kalonia DS. Application of second-derivative fluorescence spectroscopy to monitor subtle changes in a monoclonal antibody structure. *J Pharm Sci*. 2013;102(1):52–61.
54. Parak F, Frolov EN, Mossbauer RL, Goldanskii VI. Dynamics of metmyoglobin crystals investigated by nuclear gamma resonance absorption. *J Mol Biol*. 1981;145(4):825–833.
55. Doster W, Cusack S, Petry W. Dynamical transition of myoglobin revealed by inelastic neutron scattering. *Nature*. 1989;337(6209):754–756.
56. Doster W, Cusack S, Petry W. Dynamic instability of liquidlike motions in a globular protein observed by inelastic neutron scattering. *Phys Rev Lett*. 1990;65(8):1080–1083.
57. Rasmussen BF, Stock AM, Ringe D, Petsko GA. Crystalline ribonuclease A loses function below the dynamical transition at 220 K. *Nature*. 1992;357(6377):423–424.
58. Tilton Jr. RF, Dewan JC, Petsko GA. Effects of temperature on protein structure and dynamics: X-ray crystallographic studies of the protein ribonuclease-A at nine different temperatures from 98 to 320 K. *Biochemistry*. 1992;31(9):2469–2481.
59. Ferrand M, Dianoux AJ, Petry W, Zaccai G. Thermal motions and function of bacteriorhodopsin in purple membranes: effects of temperature and hydration studied by neutron scattering. *Proc Natl Acad Sci USA*. 1993;90(20):9668–9672.
60. Fitter J, Lechner RE, Dencher NA. Picosecond molecular motions in bacteriorhodopsin from neutron scattering. *Biophys J*. 1997;73(4):2126–2137.
61. Bicoût DJ, Zaccai G. Protein flexibility from the dynamical transition: a force constant analysis. *Biophys J*. 2001;80(3):1115–1123.